ADVANCED FUNCTIONAL MATERIALS

FULL PAPER

DOI: 10.1002/adfm.200800428

# Surfactant-Free, Self-Assembled PVA-Iron Oxide/Silica Core–Shell Nanocarriers for Highly Sensitive, Magnetically Controlled Drug Release and Ultrahigh Cancer Cell Uptake Efficiency**

By *Shang-Hsiu Hu, Dean-Mo Liu, Wei-Lin Tung, Chen-Fu Liao,* and *San-Yuan Chen**

Surfactant-free, self-assembled iron oxide/silica core–shell (SAIO@$SiO_2$) nanocarriers were synthesized as bifunctional magnetic vectors that can be triggered for the controlled release of therapeutic agents by an external magnetic field. In addition, drug release profiles can be well-regulated through an ultrathin layer of silica shell. The hydrophobic drug molecules were encapsulated within the iron oxide-PVA core and then further covered with a thin-layer silica shell to regulate the release pattern. Remote control of drug release from the SAIO@$SiO_2$ nanocarriers was achieved successfully using an external magnetic field where the core phase being structurally disintegrated to a certain extent while subjected to magnetic stimulus, resulting in a burst release of the encapsulated drug. However, a relatively slow and linear release restored immediately, directly after removal of the stimulus. The nanostructural evolution of the nanocarriers upon the stimulus was examined and the mechanism for controlled drug release is proposed for such a core–shell nanocarrier. Surprisingly, the surfactant-free SAIO@$SiO_2$ nanocarriers demonstrated a relatively high uptake efficiency from the HeLa cell line. Together with a well-regulated controlled release design, the nanocarriers may provide great advantages as an effective cell-based drug delivery nanosystem for biomedical applications.

## 1. Introduction

Controlled release of therapeutic agents from nanometric carriers has received increased interest because it provides numerous advantages, such as high delivery efficiency and site-specific therapy, compared to traditional dosing techniques. Owing to these advantages, many research reports propose to integrate active drug molecules with host materials, aimed at manipulating the drug release profile. It is desirable that the drug release behavior can be optimized with either a slow, zero-order release pattern or a burst-like release mimicking the natural release of biological molecules, such as the hormones insulin or thyroxine formed in endocrine glands, in the body.[1] Therefore, many studies have been published in response to specific stimuli, such as temperature,[2,3] pH,[4] electric field,[5] ultrasound,[6,7] and magnetic field[8–11] to deliver drugs in a therapeutically desirable manner. Many traditional stimuli, such as electric signals, mechanical force, pH, etc, usually needed a physical contact with the drug carriers in order to trigger drug release. However, triggering a drug release in such a manner may not be practicable in the human body. Furthermore, real-time release upon a short-time stimulus is difficult to achieve with traditional stimuli-responsive polymeric materials, this is especially critical for certain clinical complications. Therefore, development of a desired drug carrier for ''real life'' applications should possess real-time responsiveness to the stimuli, for example when urgent disease control measures are required and/or a slow, sustained release to meet different clinical complications.

Recently, iron oxide nanoparticles obtained through surface modification or combination with functional moieties have been widely used in a variety of biological applications such as drug/gene delivery,[12–15] bioseparation,[16,17] magnetic resonance imaging,[18–20] and hyperthermia therapy.[21] In contrast, there are only a limited number of reports addressed to the use of magnetic nanoparticles for controlled drug delivery. The use of a magnetic field to modulate drug release through magnetic nanoparticles from drug carriers was developed previously.[8–11] Saslawski et al. reported the use of alginated microspheres crosslinked with polyethylenenimine for pulsed release of insulin by an oscillating magnetic field.[22] The insulin release rate from the alginate-strontium ferrite microspheres was enhanced in the absence of a magnetic field. In our previous studies, a ferrogel with high-frequency magnetic field (HFMF) magnetic-sensitive properties has been characterized and the amount of drug released from the ferrogel was effectively released while applying an external magnetic field.[23] Recently, the core/single-crystal iron oxide shell nanospheres for magnetically triggered release were also developed by our

[*] Prof. S.-Y. Chen, Dr. S.-H. Hu, Prof. D.-M. Liu, Dr. W.-L. Tung, Dr. C.-F. Liao
Department of Materials Sciences and Engineering, National Chiao Tung University Hsinchu, 300 (Taiwan)
E-mail: sanyuanchen@mail.nctu.edu.tw

[**] This work was financially supported by the National Science Council of the Republic of China, Taiwan under Contract of No. NSC96-2627-B-009-006 and NSC96-2113-M009-027-MY2. Supporting Information is available online from Wiley InterScience or from the authors.

ADVANCED FUNCTIONAL MATERIALS



team. To the best of our knowledge, little investigation has so far been addressed on the controlled drug release from nanometer-sized carriers under external magnetic stimulation. However, nanocarriers with controllable drug release properties are highly desirable because such small carriers can be designed to deliver drug to a specific site of disease, and then the therapeutic molecules can be delivered at the desired location at the right time with a therapeutically effective dose. However, this is far from achievable with the current drug delivery systems, especially with particulate drug delivery nanodevices, and it seems that there is a need for a successful marriage between the field of materials technology, biology, pharmaceutics, and stimuli environment.

From a clinical point of view, it is more desirable that a ''zero or near-zero release profile'' can be tailored as practically needed before the drug-containing nanocarriers reaches the targeted sites because the nature of diffusion of drug molecules from the nanocarriers to the environment is virtually thermodynamically unavoidable in the presence of a drug concentration gradient. Once such a mechanism is triggered right after administration, the risk of undesired clinical complications may result, including a reduced therapeutic efficacy. Here, a novel nanodevice was designed and constructed by preparing self-assembled iron oxide (SAIO) nanoparticles with drug molecules embedded in an ultra-thin silica nanoshell. A structurally dense silica shell has designed as a physical barrier to eliminate undesirable drug release before reaching the target sites appears to be practically desired. A mixture of magnetic nanoparticles and amphiphilic PVA was employed as a functional phase in the resulting nanocarriers, which allows the response of the resulting drug carriers to be activated more dynamically and efficiently, aimed to achieve a real-time response to an immediate environmental change, i.e., magnetic field. In the meantime, the PVA phase provides not only a glue to assemble the nanoparticles, but also a matrix to immobilize therapeutical active agents of either hydrophilic or hydrophobic nature within. It is more interesting to know that a high-frequency magnetic field, in the range of tens to hundreds of KHz, allows a pulsed drug release to be achieved easily on a real-time responsive base without the undesirable delay in dosing accuracy under administration, and more desirably, restores to zero or near-zero release immediately after removal of the high-frequency magnetic field. In addition, the cell uptake efficiency of these novel SAIO@$SiO_2$ nanocarriers was examined.

## 2. Results and Discussion

### 2.1. Preparation of SAIO@$SiO_2$ Nanocarriers

The synthetic procedure of the SAIO@$SiO_2$ nanocarriers is schematically illustrated in Figure 1. The first step is to synthesize the monodispersed superparamagnetic iron oxide nanoparticles ($Fe_3O_4$) via high-temperature decomposition of $Fe(acac)_3$.[24] Two key steps were employed to form these monodispersed nanoparticles: firstly, the growth of nuclei was carried out at 200 °C, and then the reaction temperature was raised to 300 °C in order to permit the iron oxide nanoparticles to grow to a uniform size. The iron oxide nanoparticles showed an average diameter of 5 nm (Figure 2a) and were well suspended in benzyl ether. In the second step, the nanoemulsion method using polyvinyl alcohol (PVA) as a binder was applied to prepare the SAIO nanoparticles, Figure 2b. The iron oxide nanoparticles appeared to assemble uniformly and pack regularly throughout the PVA nanomatrix; this is believed to result from possible interactions such as hydrogen bonding or dipole-dipole interaction between the functional groups on the iron oxide surface and hydroxyl groups of the PVA, from which a PVA-induced structural alignment of the iron oxide nanoparticles can evolve. The SAIO nanoparticles having a diameter of about 77 nm, determined with dynamic light scattering (DLS, Fig. 2f), were well dispersed in aqueous solution without the need of surfactant for stabilization. Then, the SAIO was coated with a thin silica shell by hydrolysis and condensation of TEOS to obtain final core–shell SAIO@$SiO_2$ nanocarriers, Figure 2c. The SAIO@$SiO_2$ nanocarriers with a diameter of about 86 nm (Fig. 2g) possessed an ultrathin layer of dense silica shell of about 5 nm in thickness. No observable

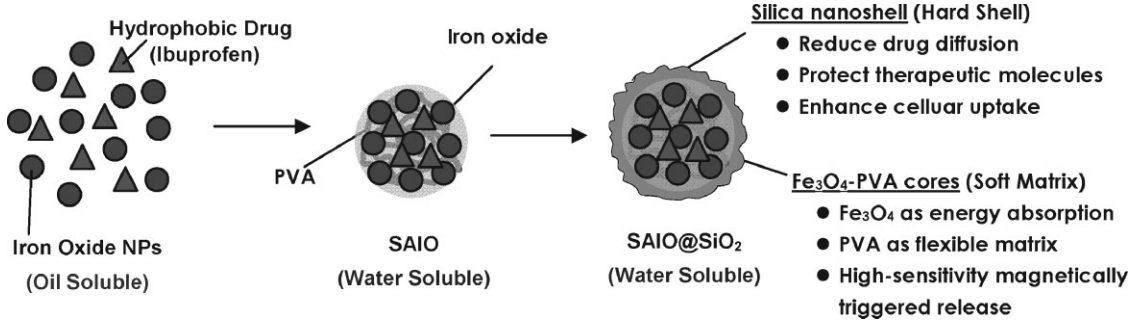


**Figure 1.** Schematic illustration of the synthesis and structure of the self-assembled iron oxide/silica core–shell (SAIO@$SiO_2$) nanocarriers for magnetically controlled drug release.

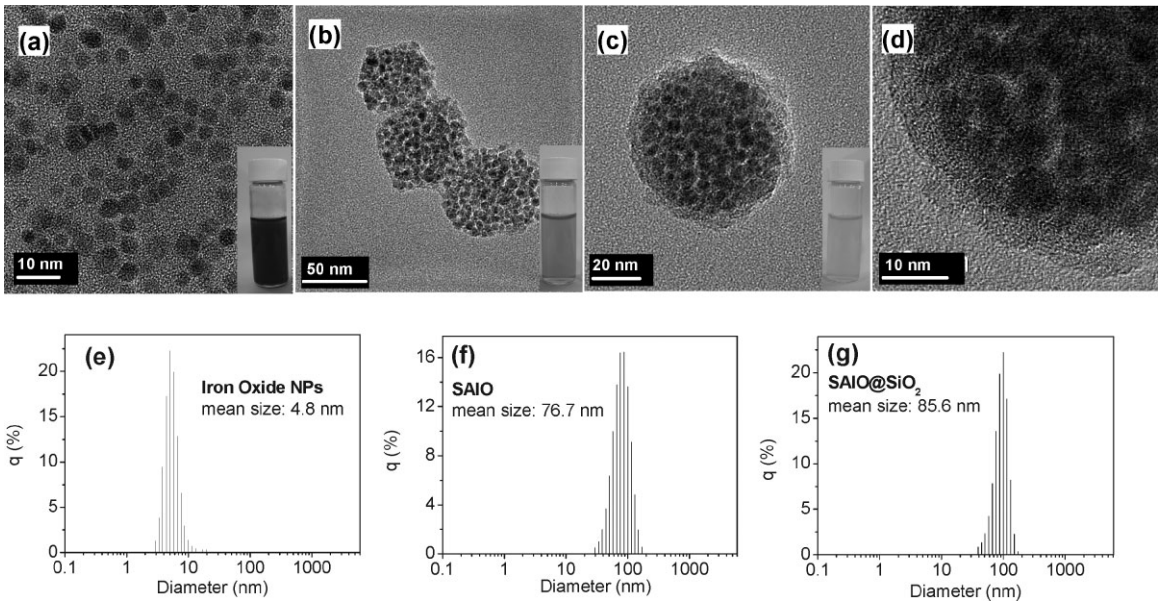


**Figure 2.** TEM images of a) iron oxide nanoparticles, b) self-assembled iron oxide (SAIO) nanospheres, and c) and d) self-assembled iron oxide/silica core–shell (SAIO@$SiO_2$) nanocarriers. The thickness of silica shells coated on the SAIO nanoparticle is 4–5 nm. The insets display the color of the solution for different particles. e)–g) The size distribution of iron oxide nanoparticles, SAIO nanoparticles, and SAIO@$SiO_2$ nanocarriers were measured by dynamic light scattering (DLS).

crevices or cracks were microscopically detectable in the regions between the SAIO and the silica shell, implying a compatible interface between the core and shell phases. The resulting core–shell nanocarriers again formed a stable suspension in both PBS solution and cell-culture solution without further chemical modification on the surface for stabilization purposes. Such a surfactant-free nanocarrier should be advantageous for many clinical practices and potential development, since it not only reduces adverse effects that may possibly originate from surfactant agents but also allows further surface modification by specific functional or biological molecules for enhanced functionality and performance, as will be further elucidated in a section below. The ultrathin silica shell was designed as a physical barrier to eliminate undesirable drug release and regulate desirable release in a controllable manner. Upon the synthesis, organic fluorescence dye was incorporated onto the silica shell through the co-condensation method for cell imaging[25] (to be discussed later).

### 2.2. Characterization of SAIO@$SiO_2$ Nanocarriers

X-ray diffraction (XRD) analysis showed that the crystalline phase of iron oxide nanoparticles is $Fe_3O_4$ (magnetite), Figure 3a. Six diffraction peaks at $2\theta = 30.1^\circ$, $35.6^\circ$, $43.3^\circ$, $53.5^\circ$, $57.2^\circ$, $62.9^\circ$ assigned as the characteristic peaks of standard $Fe_3O_4$ crystal plane were observed (according to $Fe_3O_4$ (JCPDS [85-1436]).[26] Although PVA is a semicrystalline polymer, the XRD pattern of iron oxide nanoparticles and SAIO is very similar, suggesting that the PVA/$Fe_3O_4$ ratio was negligibly small. After the SAIO was embedded by the silica layer, the relative diffraction intensity of the $Fe_3O_4$ peaks became weaker because the introduction of the silica phase diluted to a certain extent the concentration of iron oxide. In addition to the diffraction peaks of iron oxide, a broad and weak peak at $2\theta \sim 23^\circ$ was observed and identified as the semicrystalline silica. The magnetic property of $Fe_3O_4$ nanoparticles, SAIO and SAIO@$SiO_2$ nanocarriers was estimated by SQUID at 298 K with the magnetic field sweeping from $-10\,000$ to $+10\,000$ G. Figure 3b shows the correlation of the magnetization with the magnetic field for the $Fe_3O_4$ nanoparticles, SAIO and SAIO@$SiO_2$ nanocarriers, where the curves show similar shape with negligible hysteresis. The presence of PVA and silica dilutes the concentration of $Fe_3O_4$ nanoparticles, resulting in a lower saturation magnetization ($M_s$) of the SAIO and SAIO@$SiO_2$ nanocarriers than that of the pure $Fe_3O_4$ nanoparticle. The magnetic properties of the SAIO@$SiO_2$ nanocarriers were also tested by applying a magnet near the cuvette, where the SAIO@$SiO_2$ nanocarriers were completely attracted to the side of the cuvette nearest to the magnet, as displayed in Figure 3b, suggesting that the nanocarriers themselves possess magnetic properties.

### 2.3. Drug Release of SAIO and SAIO@$SiO_2$ Nanocarriers

Figure 4 shows the cumulative drug release of the SAIO and SAIO@$SiO_2$ nanocarriers in a PBS buffer solution of pH 7.4. The diagram clearly proves that both systems exhibit sustained

ADVANCED FUNCTIONAL MATERIALS



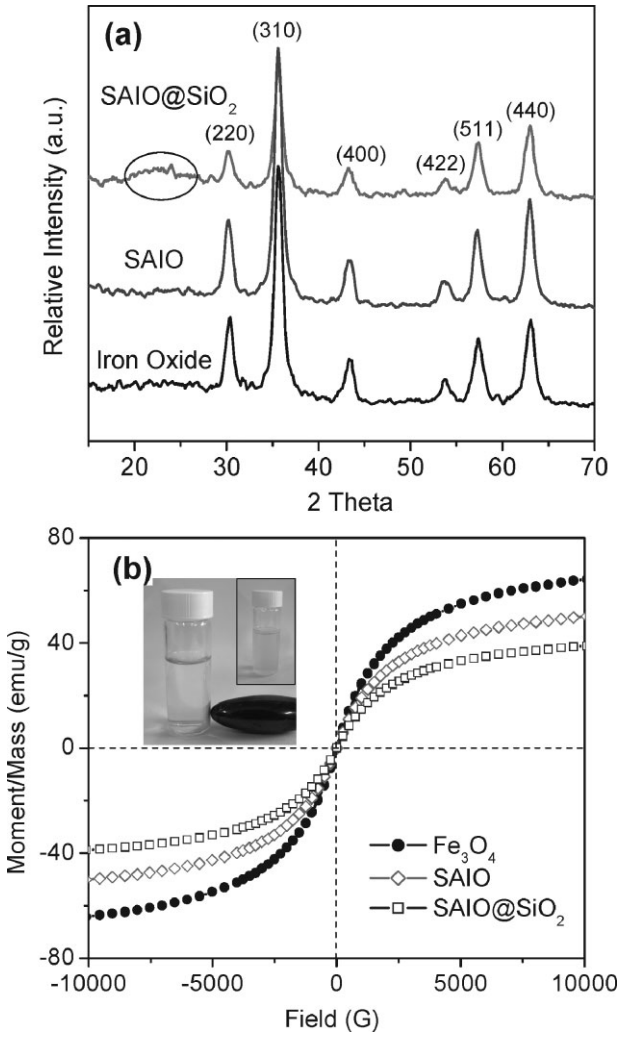


**Figure 3.** a) X-ray diffraction patterns of iron oxide nanoparticles, SAIO and SAIO@$SiO_2$. b) Field-dependent magnetization curve of iron oxide nanoparticles, SAIO and SAIO@$SiO_2$ nanocarriers. The inset shows that the SAIO@$SiO_2$ nanocarriers are attracted by an external magnet.

release behavior, but the release rates are apparently different. The amount of ibuprofen (IBU) released from the SAIO reaches 90% in 48 h; this, together with a corresponding release rate, is much higher than that from the SAIO@$SiO_2$ nanocarriers. The difference in release rate should mainly be attributed to the presence of silica shells, acting as a physical barrier, limiting the outward diffusion of the IBU. IBU, a hydrophobic drug, has limited solubility in PBS buffer so it remains readily in the SAIO. However, a concentration gradient gives rise to a driving force causing outward diffusion of the IBU through the SAIO carriers without any physical barrier to regulate the release kinetically. However, for the SAIO@$SiO_2$ nanocarriers, the release profile is highly regulated and shows a zero-order kinetic, where the rate of release is relatively slow, reaching only 8% over a time period of 48 h. This clearly indicates that the silica shell, albeit with a thickness of as small as 5 nm, acts as an effective barrier, which

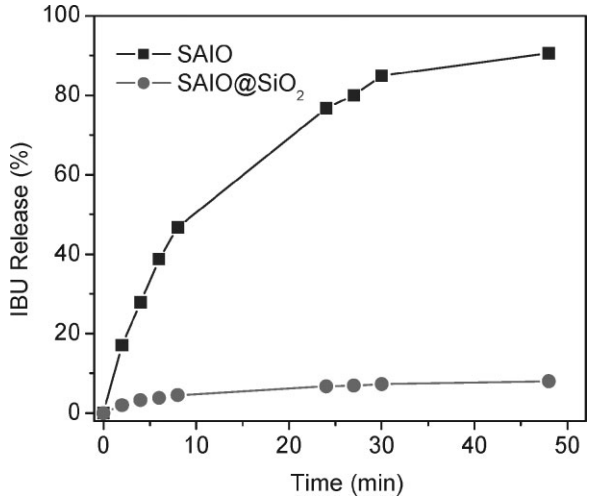


**Figure 4.** Cumulative drug release of SAIO and SAIO@$SiO_2$ nanocarriers. Coated with silica shells, the SAIO@$SiO_2$ nanocarriers exhibited a smaller amount of cumulative drug release than SAIO nanoparticles.

prevents the IBU molecules to a considerable extent from passing through. This finding also suggests that the ultrathin silica shell is structurally compact with full coverage over the entire surface of the SAIO core, as evidenced in Figure 2c, wherein no observable defects were detected along the regions of the thin shell and subsurface regions, indicating a well-compatible interface between the silica and core phase. In comparison with these two nanocarriers, the addition of an ultrathin silica shell is apparently highly capable of achieving a relatively slow release pattern, which is advantageous for preserving and protecting the drug molecules within the nanocarrier from both undesirable leakage and damage.

To investigate the diffusion mechanism of the drug from the nanocarriers, the drug release kinetics can be characterized using the equation:

$$M_t/M = kt^n,$$

where $M_t$ is the mass of drug released at time t, $M$ the mass released at infinite time, $k$ a rate constant, and $n$ is a characteristic exponent related to the mode of transport of the drug molecules.[27] The diffusion parameters (i.e., $n$ and $k$) were calculated through a log–log analysis of above equation under the condition of $M_t/M < 0.6$. The values of rate constant $k$ for the nanocarriers were then determined and found that the $k$ values decreased in the order of SAIO ($k = 0.10$) > SAIO@$SiO_2$ nanocarriers ($k = 0.01$), indicating a lower diffusion rate by a factor of 10 for the SAIO@$SiO_2$ nanocarriers. This finding strongly ascertains the efficient inhibition effect of the nanometer-sized silica shell for drug release from the SAIO@$SiO_2$ nanocarriers.

### 2.4. Magnetic-Sensitive Drug Release Behavior

Under magnetic stimulus, the release profile of IBU for both the SAIO and SAIO@$SiO_2$ nanocarriers is demonstrated in

  

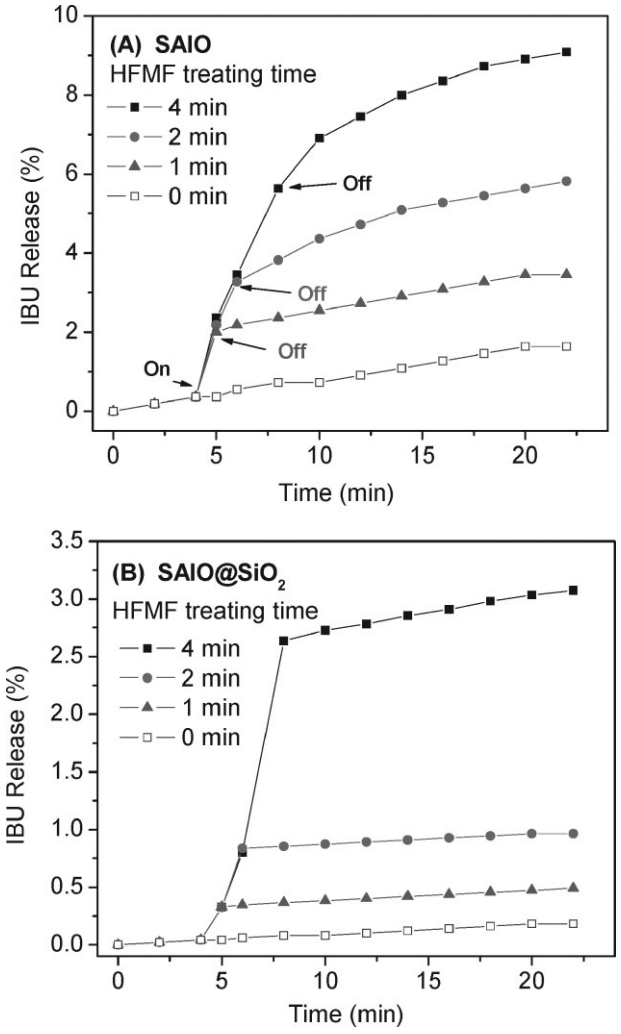


**Figure 5.** Cumulative drug release profiles of IBU from a) SAIO and b) SAIO@$SiO_2$ nanocarriers were triggered by 1 to 4 min of HFMF treatment.

Figure 5, where a significant increase in the release profile was detected for both compositions, compared to those in absence of the stimulus (Fig. 5a). For the SAIO nanoparticles, the cumulative release amount is increased from 0.4% to about 5.5% over a 4 min stimulus. The slow-to-burst release profiles were also observed while applying a consecutive magnetic stimulus at 1 min and 2 min duration. With different time durations of the stimulus, the amount of drug released from the nanocarriers showed a linear increment with the stimulus time. This finding indicates that the applied HFMF controlled the released amounts through the operation time. However, the release profile from the SAIO nanoparticles could hardly be restored right after removal of the stimulus. Moreover, the release rate was increased considerably compared to that of the as-prepared SAIO nanoparticles without subjecting to any HFMF treatment. This finding suggests that the SAIO nanoparticles can be physically and irreversibly deformed in structural integrity.

For the SAIO@$SiO_2$ nanocarriers, Figure 5b shows a slow-to-burst release profile while subjecting to HFMF, similar to the release behavior of the SAIO nanoparticles. However, a closer look at the drug release profiles of the SAIO@$SiO_2$ nanocarriers under magnetic stimulus, the cumulative release amount after 4 min period operation increased from 0.1 to 2.7%, which is smaller by a factor of 2 than that from the SAIO nanoparticles (5.5%), suggesting the silica shell effectively regulated the IBU release from the SAIO@$SiO_2$ nanocarriers. The amount of IBU from the SAIO@$SiO_2$ nanocarriers was much smaller than that from the SAIO nanoparticles. More interestingly, the release profile of the SAIO@$SiO_2$ nanocarriers possessed a zero-order release pattern, even under stimulus. In other words, the IBU released from the SAIO@$SiO_2$ nanocarriers, albeit in a burst-like profile under HFMF stimulus, can still be well regulated with a controllable dosage. When the stimulus was removed, the drug release profile immediately restored to the original pattern, i.e., to a relatively slow and zero-order release profile. Such a fast-acting and precise dosing response of the SAIO@$SiO_2$ nanocarriers relative to the given HFMF is believed to be easily achievable for practical purposes and a very promising candidate for application in magnetic-sensitive drug delivery manipulation.

### 2.5. Nanostructure Evolution under Magnetic Treatment

To investigate the release mechanism, especially under stimulus, the nanostructural evolution of the SAIO@$SiO_2$ nanocarriers subjected to HFMF was monitored, as shown in Figure 6a and b. Although the fast response to a magnetic stimulus that causes a burst release was carried out under HFMF for a 4 min duration, the nanocarriers retained their structural integrity, indicating that the drug molecules, which have a size less than 1 nm, have been accelerated considerably while passing across the silica shell. The rigid silica shell coated on the SAIO@$SiO_2$ nanocarriers acts like a framework to keep the integrity of the SAIO core phase from physical deformation or damage under extensive magnetic stimulus. Figure 6b shows that no observable cracks or defects developed on the thin silica shells, when IBU molecules were released after being subjected to HFMF treatment.

In order to estimate the structural evolution of the core phase of the SAIO@$SiO_2$ nanocarriers under the HFMF, the nanostructural evolution of the SAIO core phase without the silica shells was examined. From TEM analysis it was clear that the morphological structure of the as-synthesized SAIO nanoparticles in the absence of HFMF treatment displayed excellent structural integrity with the magnetic nanoparticles being well distributed within the PVA phase. However, after 4 min HFMF stimulus, the stresses induced by HFMF caused two types of structural deformation on the SAIO nanoparticles. First, nanocavities of 20–60 nm in size developed on the core SAIO nanoparticle, as shown in Figure 6c and d. However, some nanoparticles seemingly remained structurally

ADVANCED FUNCTIONAL MATERIALS



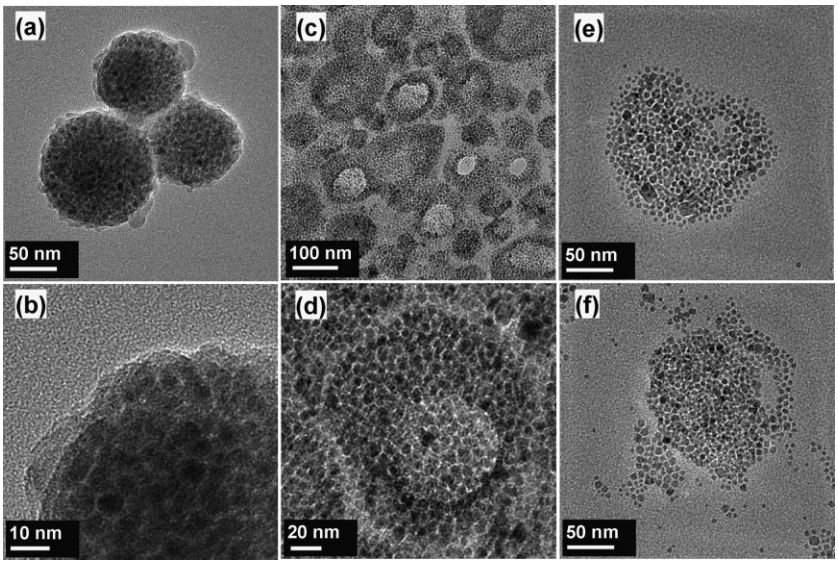


**Figure 6.** TEM images of nanostructures of a) and b) SAIO@$SiO_2$ nanocarriers, and c)–f) SAIO after 4 min duration of HFMF treatment. a) and b) SAIO@$SiO_2$ nanocarriers displayed no obviously crack after HFMF treatment. c)–f) SAIO without silica shells showed obvious cracks or deformation after applying HFMF.

intact. Second, the stress-induced serious structural deformation of the SAIO nanoparticles exhibited in Figure 6e and f. These nanocavities probably result from the dissolution of PVA in aqueous solution under magnetic-induced heating. Because the HFMF is able to induce heat energy from the magnetic nanoparticles at a faster rate, some ''hot spots'' are believed to cause structural dissociation of the SAIO core, since it is well known that heat generation, governed by the mechanism of magnetic energy dissipation for single-domain particles (Brown and Néel relaxations), is detrimental to the crystal size and the materials.[28] The temperature of the solution (5 mg $cm^{-3}$ water) will increase about 12 °C, from 24 to 36 °C. Once the energy induced by HFMF increased the temperature of SAIO nanoparticles, the PVA molecular chains became more flexible (glass transition temperature of PVA is about 80 °C), as they are subject to an aqueous and heating environment, causing the IBU molecules to diffuse more easily in the flexible and soft SAIO nanoparticles, whereupon a physical deformation of the SAIO nanoparticle was detected, as depicted in Figure 6e and f.

To investigate the weight loss of PVA after HFMF stimulus, thermogravimetric analysis (TGA) was used. After a 4 min HFMF treatment the PVA lost 7 and 2% by weight for the SAIO nanoparticles (also as a core phase for the core–shell nanocarrier) and SAIO@$SiO_2$ nanocarriers, respectively, indicating that a substantially large portion of the PVA phase still stayed within the core phase, especially for those covered with a silica shell (Table 1). However, the findings suggest that the weight loss of the PVA in the core phase is a result of outward diffusion due to the presence of surface defects such as nanopores along the silica shell. This seems to provide a reasonable explanation of the burst-like release behavior. However, what is interestingly observed from the release behavior, Figure 5b, is that the release profile followed near zero-order kinetics even under HFMF stimulus, which further substantiates that the regulating effect of the shell structure remained the same. In other words, while subjected to the HFMF, the nanostructural perturbation of the inner core phase accelerated considerably the movement of the IBU molecules due to the dissociation of the PVA phase and in the meantime, thermally induced diffusion, a significant increase in the collision frequency of the IBU to the silica shell by a factor of est. 10 was observed. In consequence, a burst-like release behavior for the SAIO@$SiO_2$ nanocarrier was detected. However, once the stimulus was removed, the inner core phase must restore rapidly to original status, where the PVA solidified and thermal perturbation due to superparamagnetic nature of the nanometer-sized iron oxide nanoparticles ceased. The nanostructural integrity of the silica shell remained intact, where the regulating effect kept identically effective, as evidenced in the release profiles upon several ''on–off'' operations, Figure 5b.

Mechanical motion of iron oxide nanoparticles within the core phase under HFMF gives rise to an alternative contribution to the burst-release pattern of the SAIO@$SiO_2$ nanocarriers. The degree and speed of deformation of the SAIO core phase depended on the interactions among the nanomagnets and PVA phase, where both phases are in intimate contact within a nanometric confinement. Magnetic nanoparticles in the magnetic field stretch along the field direction due to the magnetostatic energy:

$$E_{ms} = 1/2(N_{\parallel} - N_{\perp})M^2V \quad (1)$$

where $N_{\parallel}$ and $N_{\perp}$ are demagnetizing factors in the directions parallel and perpendicular to the magnetic field. $E_{ms}$ is the energy of magnetic interaction of the magnetic moment $M$ of the nanoparticles with magnetic field $H$. $V$ is the volume of magnetic nanoparticles.[11] While applying a magnetic field,

**Table 1.** TGA analysis of SAIO and SAIO@$SiO_2$ nanospheres before and after a 4 min HFMF treatment.

| Sample | Inorganic [wt %] | Organic (PVA) [wt %] | PVA Lost [%] |
|---|---|---|---|
| SAIO@SiO2-HF4 | 84.3 | 15.7 | ~2 |
| SAIO@SiO2 | 84 | 16 | – |
| SAIO-HF4 | 80.5 | 19.5 | ~7 |
| SAIO | 79 | 21 | – |

magnetostatic interactions induced by the magnetic field will cause the appearance of a demagnetizing field inside the SAIO core. Owing to this magnetostatic interaction, the magnetic particles in the core phase will tend to move, resulting in establishing stresses inside the nanostructures. Such stresses may act a factor accelerating the formation of the nanocavities and deformation of SAIO nanoparticles as shown in Figure 6c to f. From experimental observations, it suggests that such a HFMF-induced nanostructural evolution involves the following four stages: (i) heating of the SAIO core locally, (ii) causing a certain degree of relaxation of polyvinyl alcohol that further combines with (iii) the mechanical motions of iron oxide nanoparticles, following (iv) defect formation, which is especially pronounced for SAIO nanoparticles. Such a nanostructural evolution under HFMF stimulus surely enhances the burst release behavior from within the core phase for the SAIO@$SiO_2$ nanocarriers.

### 2.6. Cell Uptake

Cellular uptake of the FITC-labled SAIO@$SiO_2$ nanocarriers was investigated by PL microscopy and flow cytometry. After 24 h of HeLa cell incubation, which is employed as a cancer cell model, cells treated with FITC-SAIO@$SiO_2$ nanocarriers for various time durations were monitored. Figure 7a–d shows that the nanocarriers subjected to the cells with an exposure time varying from 30 min to 4 h were gradually uptaken by the cells, probably through endocytosis. The green fluorescence dye can clearly be observed in the cytoplasm. The green FITC nanocarriers appear localized as discrete dots suggesting that the nanocarriers do not show any detectable leaching. For an incubation time of 30 min, some of the nanocarriers appeared to attach rapidly on the surface of the cell membranes, Figure 7a, and this further increases for a 1 h incubation, Figure 7b, showing that a large amount of the labeled nanocarriers adsorbed onto the cells and some appeared to be residing in the cells. Figure 7c shows that after 2 h of incubation the nanocarriers largely migrate to the cytoplasm region, where some light spots can be clearly visually detected in their cytoplasm. With 4 h of incubation, considerable regions of the cytoplasm displayed strong green fluorescence illuminance, as shown in Figure 7d, indicating that the nanocarriers are efficiently localized within the cell. It is also illustrated a relatively fast cellular uptake efficiency for the SAIO@$SiO_2$ nanocarriers, the absence of un-desirable surfactant and highly biocompatible, textured silica shell may take responsible for such an ultra-fast cell uptake behavior.

Figure 8a shows the results of the MTT (3-(4,5-dimethyldiazol-2-yl)-2,5 diphenyl Tetrazolium Bromide) assay, which represents a measure of metabolic competence of the cell with SAIO and SAIO@$SiO_2$ nanospheres for different concentrations. The difference in the cytotoxicity at 12 to 48 h of incubation is negligibly small. At a highest concentration of 5 $\mu L\ cm^{-3}$ SAIO, the cell viability also remained at about 100%. The results suggest that the microcapsules were low in toxicity with respect to the HeLa cell line. Flow cytometric spectra, Figure 8b, also indicate that the FITC-SAIO@$SiO_2$ nanocarriers are capable of penetrating the HeLa cells efficiently. Although flow cytometry cannot clearly define the surface-bound and intracellular nanocarriers, the PL image strongly suggests that the nanocarriers are largely being uptaken by the cancer cells over a relatively short contact time. With increasing incubation time of the nanocarriers, i.e., from 30 min to 2 h, the fluorescence intensity measured by flow cytometry increased proportionally, further indicating that cellular uptake of the FITC-SAIO@$SiO_2$ nanocarriers can occur efficiently and rapidly. This finding indicates that the SAIO@$SiO_2$ nanocarriers showed little cytotoxicity to the HeLa cells, suggesting excellent biocompatibility and should accordingly be highly compatible with healthy cells. As a critical requirement for anti-cancer drug delivery strategy, reduction of the cytotoxicity of the drug carrier itself can be achieved and a further minimization of the cytotoxicity of the drug can be

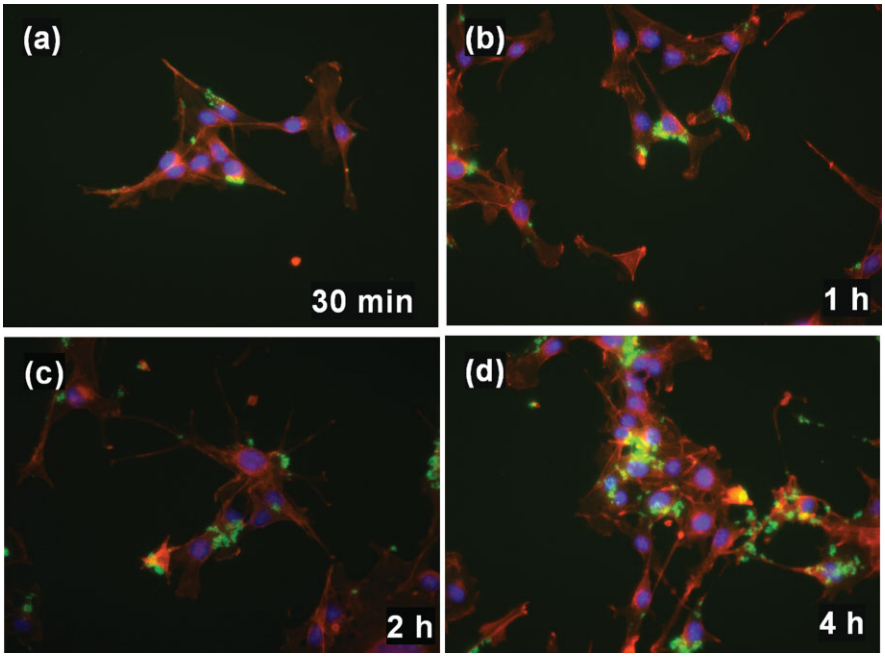


**Figure 7.** Time-course PL microscopy images of HeLa cells labeled with FITC-SAIO@$SiO_2$ nanocarriers, the cell skeleton wsa stained with rhodamine phalloidin (red), and cell nucleus with DAPI (purple). Cells were incubated with FITC-SAIO@$SiO_2$ nanocarriers for a) 30 min, b) 1 h, c) 2 h, and d) 4 h.

ADVANCED FUNCTIONAL MATERIALS



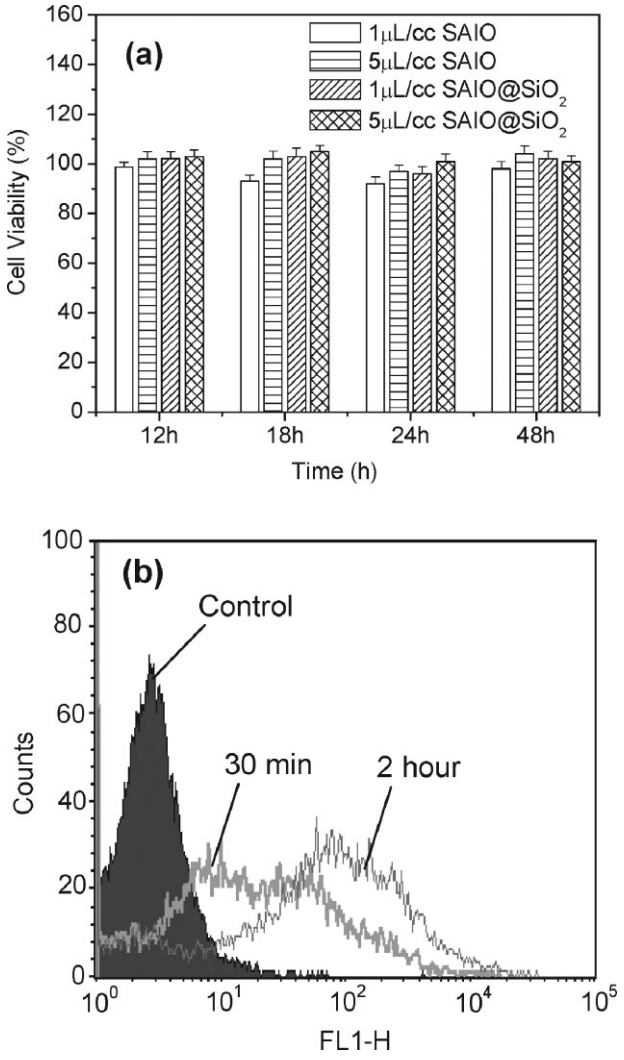


**Figure 8.** a) Cell viability of HeLa cells after 12 to 48 h of incubation with increasing amounts of SAIO and SAIO@$SiO_2$ nanospheres. Cell viability was measured using an MTT assay. b) Flow cytometry analysis for the FITC-SAIO@$SiO_2$ nanocarriers accumulated in HeLa cells for incubation of 30 min and 2 h.

obtained as well. To our surprise, the ultra-fast cellular uptake of the nanocarriers occurred within dozens of minutes, which, associated with a rapid and precise dosing corresponding to an external stimulus, provides a pathway for cellular-based, controlled drug delivery and also offers potential advantages for application in cellular imaging.

## 3. Conclusions

Self-assembled iron oxide/silica core–shell (SAIO@$SiO_2$) nanocarriers were fabricated as multifunctional drug vectors. The core–shell nanocarriers are able to well-disperse easily in an aqueous solution without using any interfacial molecules for stabilization, which provides great advantages for practical medical uses such as forming a suspension for injection or oral administrations. The ultrathin, 4–5 nm, outer silica shell coated on the SAIO core, a mixture of iron oxide nanoparticles and PVA, blocked the drug molecules effectively from therapeutically undesirable release from the core phase before subjecting to magnetic stimulation. Under HFMF treatment, the SAIO@$SiO_2$ nanocarriers displayed a fast-acting and precise stimulus-time-dependent dosing response to the environment and restored to the original state, i.e., a relatively slow and zero-order release profile, immediately after removal of the stimulus. In addition, the surfactant-free SAIO@$SiO_2$ nanocarriers were allowed a high efficiency uptake by HeLa cells within dozens of minutes and have been shown to exhibit excellent cytocompatibility, implying the nanocarriers are potentially capable of offering highly efficient, cellular-based delivery following a fast-acting, accurate release of therapeutic agents for anti-cancer applications.

## 4. Experimental

*Materials*: The synthesis was carried out under airless conditions and using commercially available reagents. Absolute ethanol (99.5%), benzyl ether (99%), 1,2-hexadecanediol (97%), oleic acid (90%), oleylamine (>70%) and Iron(III) acetylacetonate were purchased from Aldrich Chemical Co. Polyvinyl alcohol (PVA, $M_w$: 72*k*) were purchased from Fluka Chemical Co. Tetraethylorthosilicate (TEOS) and 3-aminopropyltrimethoxy silane (APTMS) were purchased from Merck. Fluorescein isothiocyanate (FITC, Sigma) were used to label, which help nanocarrier visualization under a fluorescence microscope. Ibuprofen (IBU, Fluka) was used as the model drug.

*Synthesis of Magnetic Nanoparticles*: Monodisperse iron oxide nanoparticles were synthesized by a method developed by Sun et al. [24]. Briefly, 5 nm of iron oxide nanoparticles were synthesized by mixing 2 mmol $Fe(acac)_3$ (iron III acetylacetonate), 10 mmol 1,2-dodecanediol, 6 mmol oleic acid, 6 mmol oleylamine, and 20 mL benzyl ether under a flow of nitrogen. The mixture was stirred magnetically and preheated to reflux (200 °C) for 30 min, and then, heated to 300 °C for another 1 h under nitrogen atmosphere. The black-brown mixture was allowed to cool to room temperature and added 50 mL ethanol to participate. The products were collected by centrifugation at 6 000 rpm for 10 min and then 4 times washed with an excess of pure ethanol. The product, iron oxide nanoparticles, was centrifuged to remove solvent, and redispersed into hexane.

*Synthesis of Self-Assembled Iron-Oxide Nanoparticles/Silica Core–Shell (SAIO@$SiO_2$) Nanocarriers*: To prepare self-assembly iron oxide nanoparticles (SAIO), 10 mg of iron oxide nanoparticles were centrifuged at 6 000 rpm for 10 min, and then redispersed in 4 mL chloroform to form an uniform organic phase. 200 mg of polyvinyl alcohol (PVA) as a polymer binder was dissolved in 10 mL de-ionized (DI) water at 70 °C. After PVA has been totally dissolved in the solution, the clear solution was cooled to room temperature. Then, organic phase was added into the PVA solution. The mixture was emulsified for 5 min with an ultrasonicator at 100 W. Under the ultrasonicating, the mixture was heated and evaporated the organic solvent. The mixture was stirred magnetically and heated again to 50 °C on a hot plate to ensure removal of the organic phase. After evaporation of the organic solvent, the products were washed 3 times with DI water and then centrifuged at 6 000 rpm to collect the products. The precipitates were redispersed in water; the diameter of the redispersed particles (hereinafter termed as SAIO) was about 77 nm.

Once the solvent was removed, a mixture of PVA and iron oxide nanoparticles was formed where the iron oxide nanoparticles appeared to assemble in a somewhat uniform and regular configuration in the resulting SAIO phase. An ultrathin silica shell was then coated on the SAIO nanoparticles by a modified Stöber method. In brief, 5 mg of SAIO were dispersed in 4 mL of 99.5% ethanol and 0.1 mL of 33% $NaOH_4$ for 30 min. 40 μm of tetraethylorthosilicate (TEOS) was slowly added to the mixture and stirred for 12 h. After hydrolysis and condensation, a silica nanoshell was coated on the SAIO nanoparticle to form the resulting PVA/iron oxide/silica core–shell (termed as SAIO@$SiO_2$) nanocarriers.

*Characterization*: The morphology of iron oxide nanoparticles, SAIO nanoparticles, and SAIO@$SiO_2$ nanocarriers were examined using field emission scanning electron microscopy (FE-SEM, JEOL-6500, Japan) and transmission electron microscopy (TEM, JEM-2100, Japan). For SEM analysis, the nanocarriers were dried on the 0.5 cm × 0.5 cm silicon waters. After drying, the microcapsules were coated with an ultrathin metal layer through the platinum sputtering to enhance the image quality taken in the experiments. X-ray diffractometer (XRD, M18XHF, Mac Science, Japan) was used to identify the crystallographic phase of iron oxide nanoparticles and magnetic nanospheres, at a scanning rate of 6 ° $2\theta$ per min over a range of $2\theta$ from 10 ° to 70 °. The magnetization of the SAIO@$SiO_2$ nanocarriers was measured by a superconducting quantum interference device (SQUID, MPMS-XL7) at 298 K and ±8000 G applied magnetic field. Before SQUID analysis, the iron oxide nanoparticles and microcapsules were dried in the vacuum oven for 60 °C for 2 d. A high-frequency magnetic field (HFMF) was produced by a power supply, functional generator, amplifier, and cooling water. The strength of the magnetic field depended on the coils. In this study, the coil was 8 loops, frequency 50 kHz and the strength of the magnetic field ($H$) 2.5 kA $m^{-1}$. The temperature of HFMF generator was controlled by cycling cooling water at 25 °C.

*Drug Loading and Release*: In this investigation, IBU was used as a model drug to estimate the drug release behaviors of the SAIO@$SiO_2$ nanocarriers, loading in nanocarriers through an in situ process. First, 4% IBU was dissolved in chloroform with iron oxide nanoparticles to form the organic phase. This organic phase was used to prepare the SAIO nanoparticles. IBU can be encapsulated in the SAIO nanoparticles through amphiphilic polyvinyl alcohol (PVA). Then, the process of constructing SAIO and silica shells was also applied to prepare drug-loading SAIO@$SiO_2$ nanocarriers. Before the drug release test, the nanocarriers were washed with a phosphate buffered saline (PBS) solution (pH 7.4), following by washing with DI water. IBU-containing nanocarriers were used in PBS buffer solution for all the drug-release experiments. A quantitative estimate of IBU loading was obtained by UV–vis spectrophotometry. The drug release behavior from the nanocarriers was measured in a 20 mL PBS solution per sponge cube (pH 7.4). To measure the concentration of the drug release, 1.5 mL PBS medium with the dispersed nanospheres was taken out, and separated by centrifugation at 4 000 rpm. The clear solution without the nanospheres was used to estimate the concentration of drug release UV–vis spectroscopy (Agilent, 8453 1UV-Visible spectrophotometer) was used for characterization of absorption peak at 264 nm ($I_{max}$ of free IBU). The nanocarriers were absent and did not affect the measurements.

*Cell Culture*: HeLa (human cervical cancer) cells were maintained in DMEM (Dulbecco's modified Eagle's medium) containing 10% fetal bovine serum, 100 units/mL penicillin, and 100 μg $mL^{-1}$ streptomycin. Cells were cultured with complete medium at 37 °C in a humidified atmosphere of 5% $CO_2$ in air. For all experiments, cells were harvested from sub-confluent cultures by use of trypsin and were resuspended in fresh complete medium before plating. A comparison of in vitro cytotoxicity of SAIO@$SiO_2$ nanocarriers with different concentrations and times was performed on HeLa cells with an in vitro proliferation method using MTT [50]. Briefly, $1 \times 10^4$ cells were plated in 96-well plates to allow the cells to attach and then exposed to the serial concentrations of SAIO@$SiO_2$ nanocarriers at 37 °C. At the end of the incubation, 20 μL of MTT solution was added and incubated for another 4 h. Then, the medium was replaced with 200 μL of DMSO and the absorbance was monitored using a Sunrise absorbance microplate reader at dual wavelengths of 570 and 650 nm.

In order to estimate the cellular uptake of the nanocarriers, green-emitting fluorescein dye was attached SAIO@$SiO_2$ nanocarriers (FITC-SAIO@$SiO_2$) for the study. First, fluorescein isothiocyanate (FITC) was mixed with ethanolic 3-aminopropyltrimethoxysilane (APTMS) solution for 24 h at room temperature to form *N*-1-(3-trimethoxysilylpropyl)- N-fluoresceyl thiourea (FITC-APTMS). Separately, 5 mg of SAIO were dispersed in 4 mL of 99.5% ethanol and 0.1 mL of 33% NaOH for 30 min. 40 μm Tetraethylorthosilicate (TEOS) and 10 μm FITC-APTMS was slowly added to the mixture and then stirred for 12 h. After hydrolysis and condensation, the FITC-silica was coated on the SAIO to form FITC-SAIO@$SiO_2$ nanocarriers. The unreacted chemicals were removed by rinsed with DI water for 3 times. The SAIO@$SiO_2$ nanocarriers were incubated with the cells for different periods of time and then studied by PL microscopy.

Received: March 26, 2008
Revised: May 23, 2008
Published online: September 22, 2008

[1] A. C. R. Grayson, I. S. Choi, B. M. Tyler, P. P. Wang, H. Brem, M. J. Cima, R. Langer, *Nat. Mater.* **2003**, *2*, 767.
[2] Z. Hu, X. Xia, *Adv. Mater.* **2004**, *16*, 305.
[3] X. Z. Zhang, D. Q. Wu, C. C. Chu, *Biomaterials* **2004**, *25*, 3793.
[4] M. Das, S. Mardyani, W. C. W. Chan, E. Kumacheva, *Adv. Mater.* **2006**, *18*, 80.
[5] M. R. Abidian, D. H. Kim, D. C. Martin, *Adv. Mater.* **2006**, *18*, 405.
[6] B. G. De Geest, A. G. Skirtach, A. A. Mamedov, A. A. Antipov, N. A. Kotov, S. C. De Smedt, G. B. Sukhorukov, *Small* **2007**, *3*, 804.
[7] H. J. Kim, H. Matsuda, H. Zhou, I. Honma, *Adv. Mater.* **2006**, *18*, 3083.
[8] E. R. Edelman, J. Kost, H. Bobeck, R. Langer, *J. Biomed. Mater. Res.* **1985**, *19*, 67.
[9] J. Kost, J. Wolfrum, R. Langer, *J. Biomed. Mater. Res.* **1987**, *21*, 1367.
[10] J. Kost, R. Noecker, E. Kunica, R. Langer, *J. Biomed. Mater. Res.* **1985**, *19*, 935.
[11] Z. vLu, M. D. Prouty, Z. Guo, V. O. Golub, C. S. S. R. Kumar, Y. M. Lvov, *Langmuir* **2005**, *21*, 2042.
[12] U. Schillinger, T. Brill, C. Rudolph, S. Huth, S. Gersting, F. Krötz, J. Hirschberger, C. Bergemann, C. Plank, *J. Magn. Magn. Mater.* **2005**, *293*, 501.
[13] A. S. Lübbe, C. Bergemann, J. Brock, D. G. McClure, *J. Magn. Magn. Mater.* **1999**, *194*, 149.
[14] T. Neuberger, B. Schöpf, H. Hofmann, M. Hofmann, B. von Rechenberg, *J. Magn. Magn. Mater.* **2005**, *293*, 483.
[15] T. J. Yoon, J. S. Kim, B. G. Kim, K. N. Yu, M. H. Cho, J. K. Lee, *Angew. Chem. Int. Ed.* **2005**, *44*, 1068.
[16] I. Koh, X. Wang, B. Varughese, L. Isaacs, S. H. Ehrman, D. S. English, *J. Phys. Chem. B* **2006**, *110*, 1553.
[17] P. S. Doyle, J. Bibette, A. Bancaud, J. L. Viovy, *Science* **2002**, *295*, 2237.
[18] O. Veiseh, C. Sun, J. Gunn, N. Kohler, P. Gabikian, D. Lee, N. Bhattarai, R. Ellenbogen, R. Sze, A. Hallahan, J. Olson, M. Zhang, *Nano Lett.* **2005**, *5*, 1003.
[19] C. W. Lu, Y. Hung, J. K. Hsiao, M. Yao, T. H. Chung, Y. S. Lin, S. H. Wu, S. C. Hsu, H. M. Liu, C. Y. Mou, C. S. Yang, D. M. Huang, Y. C. Chen, *Nano Lett.* **2007**, *7*, 149.
[20] Y. M. Huh, Y. W. Jun, H. T. Song, S. Kim, J. S. Choi, J. H. Lee, Y. Yoon, K. S. Kim, J. S. Shin, J. S. Suh, J. Cheon, *J. Am. Chem. Soc.* **2005**, *127*, 12387.

ADVANCED FUNCTIONAL MATERIALS



[21] A. Jordan, R. Scholz, P. Wust, H. Schirra, T. Schiestel, H. Schmidt, R. Felix, *J. Magn. Magn. Mater.* **1999**, *194*, 185.
[22] O. Saslawski, C. Weingarten, J. P. Benoit, P. Couvreur, *Life Sci.* **1988**, *42*, 1521.
[23] S. H. Hu, T. Y. Liu, D. M. Liu, S. Y. Chen, *Macromolecules* **2007**, *40*, 6786.
[24] S. Sun, H. Zeng, D. B. Robinson, S. Raoux, P. M. Rice, S. X. Wang, G. Li, *J. Am. Chem. Soc.* **2004**, *126*, 273.
[25] Y. S. Lin, C. P. Tsai, H. Y. Huang, C. T. Kuo, Y. Hung, D. M. Huang, Y. C. Chen, C. Y. Mou, *Chem. Mater.* **2005**, *17*, 4570.
[26] J. W. Long, M. S. Logan, C. P. Rhodes, E. E. Carpenter, R. M. Stroud, D. R. Rolison, *J. Am. Chem. Soc.* **2004**, *126*, 16879.
[27] P. L. Ritger, N. A. Peppas, *J. Controlled Release* **1987**, *5*, 37.
[28] J. P. Fortin, C. Wilhelm, J. Servais, C. Ménager, J. C. Bacri, F. Gazeau, *J. Am. Chem. Soc.* **2007**, *129*, 2628.